6-3-2013

Evaluation of a Coupled Event-driven Phenology and Evapotranspiration Model for Croplands in the United States Northern Great Plains

V. Kovalskyy
South Dakota State University

G. M. Henebry
South Dakota State University

D. P. Roy

B. Adusei

M. Hansen

See next page for additional authors

Authors

V. Kovalskyy, G. M. Henebry, D. P. Roy, B. Adusei, M. Hansen, G. Senay, and D. M. Mocko

Evaluation of a coupled event-driven phenology and evapotranspiration model for croplands in the United States northern Great Plains

V. Kovalskyy,[1] G. M. Henebry,[1] D. P. Roy,[1] B. Adusei,[1,4] M. Hansen,[1,4] G. Senay,[2] and D. M. Mocko[3]

[1]   A new model coupling scheme with remote sensing data assimilation was developed for estimation of daily actual evapotranspiration (ET). The scheme consists of the VegET, a model to estimate ET from meteorological and water balance data, and an Event Driven Phenology Model (EDPM), an empirical crop specific model trained on multiple years of flux tower data transformed into six types of environmental forcings that are called "events" to emphasize their temporally discrete character, which has advantages for modeling multiple contingent influences. The EDPM in prognostic mode supplies seasonal trajectories of normalized difference vegetation index (NDVI); whereas in diagnostic mode, it can adjust the NDVI prediction with assimilated remotely sensed observations. The scheme was deployed within the croplands of the Northern Great Plains. The evaluation used 2007–2009 land surface forcing data from the North American Land Data Assimilation System and crop maps derived from remotely sensed data of NASA's Moderate Resolution Imaging Spectroradiometer (MODIS). We compared the NDVI produced by the EDPM with NDVI data derived from the MODIS nadir bidirectional reflectance distribution function adjusted reflectance product. The EDPM performance in prognostic mode yielded a coefficient of determination (r^2) of 0.8 ± 0.15 and the root mean square error (RMSE) of 0.1 ± 0.035 across the entire study area. Retrospective correction of canopy attributes using assimilated MODIS NDVI values improved EDPM NDVI estimates, bringing the errors down to the average level of 0.1. The ET estimates produced by the coupled scheme were compared with the MODIS evapotranspiration product and with ET from NASA's Mosaic land surface model. The expected $r^2 = 0.7 \pm 0.15$ and RMSE = 11.2 ± 4 mm per 8 days achieved in earlier point-based validations were met in this study by the coupling scheme functioning in both prognostic and retrospective modes. Coupled model performance was diminished at the periphery of the study area where r^2 values were about 0.5 and RMSEs up to 15 ± 5 mm per 8 days. This performance degradation can be attributed both to insufficient EDPM training and to spatial heterogeneity in the accuracy of the crop maps. Overall, the experiment provided sufficient evidence of soundness of the EDPM and VegET coupling scheme, assuring its potential for spatially explicit applications.

[1]South Dakota State University Geographic Information Science Center of Excellence, Brookings, South Dakota, USA.

[2]United States Geological Survey Center for Earth Resources Observation and Science, Sioux Falls, South Dakota, USA.

[3]SAIC at the Hydrological Sciences Laboratory and the Global Modeling and Assimilation Office, NASA Goddard Space Flight Center, Greenbelt, Maryland, USA.

[4]Now at Department of Geographical Sciences, University of Maryland, College Park, Maryland, USA.

Corresponding author: V. Kovalskyy, South Dakota State University Geographic Information Science Center of Excellence, Brookings, South Dakota, USA. (Valeriy.Kovalskyy@sdstate.edu)

1. Introduction

[2]   There is growing consensus in the climate science community that the ability to precisely partition energy and matter fluxes on the land surface is key to improving our understanding of mesoscale atmospheric dynamics, ecosystem responses to climate change, and interactions with human activities [*Pitman*, 2003; *Ibanez et al.*, 2010; *Niu et al.*, 2011]. Since *Manabe* [1969] researchers have been coupling global and regional climate models with land surface models (LSM) to model interactions between the land surface and the lower levels of the atmospheric boundary layer. Among many surface fluxes, LSMs keep track of actual evapotranspiration (ET_a) that quantifies surface water loss to evaporation from

land surface and plant transpiration. Vegetation cover poses a major challenge for ET_a modeling due to its spatial and temporal variability, and therefore, various process-based [*Lawrence and Chase*, 2007; *Sabater et al.*, 2008; *Wegehenkel*, 2009; *Vinukollu et al.*, 2011; *Yan et al.*, 2012] and empirical methods [*Nagler et al.*, 2005; *Godfrey et al.*, 2007; *Senay et al.*, 2007; *Jang et al.*, 2009; *Li et al.*, 2009; *Gao et al.*, 2010; *Zhenzhong et al.*, 2012] have been used to incorporate vegetation cover. Model parameterization of croplands is particularly challenging because crop temporal dynamics, irrigation regimes, and diverse agricultural practices can have complex effects on evapotranspiration [*Pitman*, 2003; *Abramowitz et al.*, 2008].

[3] The use of fully functional crop models as alternatives of LSMs in field scale studies to assess regional agricultural developments has been a common practice [*Maruyama and Kuwagata*, 2010; *Stancalie et al.*, 2010]. However, many study cases require spatially explicit ET_a estimates over larger areas. This requirement would entail additional parameterization, tuning, and running time for the models like ALMANAC [*Debaeke et al.*, 1997; *Kiniry et al.*, 2008], CERES [*Mearns et al.*, 1999; *Liu et al.*, 2011], CROPWAT [*Stancalie et al.*, 2010; *Nkomozepi and Chung* 2012], or MODWht [*Kang et al.*, 2009]. Deployment of several of these models in a spatially explicit study of evapotranspiration dynamics in croplands may result in numerous parameterization conflicts and computational constraints [*Iglesias et al.*, 2011]. Therefore, a simplified simulator of ET_a called VegET [*Senay* 2008] coupled with a multicrop vegetation model can potentially be a solution for finer spatial resolution studies where multiple crops are grown within one mapping unit. A key advantage of VegET is the modulation of reference evapotranspiration by a canopy phenology coefficient derived from the normalized difference vegetation index (NDVI) [*Tucker*, 1979], which has been used as a proxy for numerous canopy properties important for ET and other surface fluxes [*Dickinson et al.* 1998; *Foley et al.* 2000; *Godfrey et al.* 2007; *Prihodko et al.* 2008; *Rosero et al.* 2009; *Rötzer et al.* 2010; *Zha et al.* 2010]. The original implementation of VegET used climatologies of NDVI as canopy phenology parameters. However, the climatologies would not reflect changes in growing conditions [*Godfrey et al.*, 2007; *Wegehenkel*, 2009] or changes in crop areas. Therefore, the NDVI climatologies were replaced with an interactive vegetation growth module Event Driven Phenology Model (EDPM) [*Kovalskyy and Henebry*, 2012a] capable of predicting seasonal daily NDVI trajectories. The EDPM can predict daily NDVI independently when working in prognostic mode. The model can also assimilate satellite observations to correct its NDVI predictions retrospectively when working in diagnostic mode. The coupled EDPM-VegET scheme has a potential not only in phenological or crop modeling applications but also for monitoring vegetation and evapotranspiration.

[4] This paper presents temporally and spatially explicit validation of the coupled EDPM-VegET scheme that models seasonal dynamics of NDVI and evapotranspiration. Previously, the EDPM has been shown, at a small number of U.S. flux towers, to capture fine temporal details of crop NDVI dynamics and provide canopy phenology parameterization for VegET [*Kovalskyy and*

Henebry, 2012b]. Similarly, the EDPM is used in this study to parameterize VegET in a regional application to estimate daily actual evapotranspiration during the growing seasons of 2007, 2008, and 2009. The spatially explicit NDVI was modeled by the EDPM using meteorological forcings and, for this paper, by satellite-derived annual crop cover maps covering more than 0.5 million km^2 of the United States Northern Great Plains. The EDPM was run in prognostic mode to predict daily NDVI during the growing season, and in diagnostic mode where the predicted NDVI are corrected via a data assimilation scheme using near-weekly NDVI derived from Moderate Resolution Imaging Spectroradiometer (MODIS) data.

[5] The analysis is focused on three aspects of the EDPM and the VegET model performance. First, temporal and spatial differences between the EDPM NDVI estimates and NDVI values derived from MODIS are analyzed. Second, the EDPM-derived phenological dates defining the start, end, and length of the growing season are compared with comparable phenological dates derived from the weekly Crop Progress reports of the U.S. National Agricultural Statistics Service (NASS). Third, the ET_a results derived from the coupled EDPM-VegET model are compared with contemporaneous MODIS and Mosaic ET_a products.

2. Methods and Materials

2.1. Study Area

[6] The study area encompasses all of Nebraska, Iowa, Minnesota, North Dakota, South Dakota, and parts of Illinois and Indiana. Together, these states include more than half of the nation's maize and soybean crops and comprise the major part of the U.S. maize and soybean belts [*Chang et al*, 2007]. Within these states, only $0.05°$ grid cells with at least 50% maize or soybean cover mapped in any of 2007, 2008, or 2009 were considered (Figure 1). Maize and soybean are the most prevalent crops across the region. Farmers use different genetic varieties of these crops to match the growing conditions of their farms and to spread production risk [*Ransom et al.*, 2004]. The green-up of the area generally starts in early May in the southeast and can be as late as mid-June in the northwest. The length of the growing cycle also varies greatly from almost 5 months in the south to slightly more than 3 months in the north. The growing season across the region is always within the period March to October. There are strong ET gradients across the region, from 600 mm ET annually in the North to 1000 mm in the South, and as low as 400 mm at the western extreme [*Willmott and Matsuura*, 2007].

2.2. Modeling

[7] The model coupling scheme evaluated in this paper consists of two parts: the VegET model [*Senay*, 2008] to estimate ETa from meteorological and water balance data and the EDPM, an empirical crop specific model trained on flux tower data and capable of producing seasonal trajectories of NDVI and drive canopy phenology coefficient in the VegET.
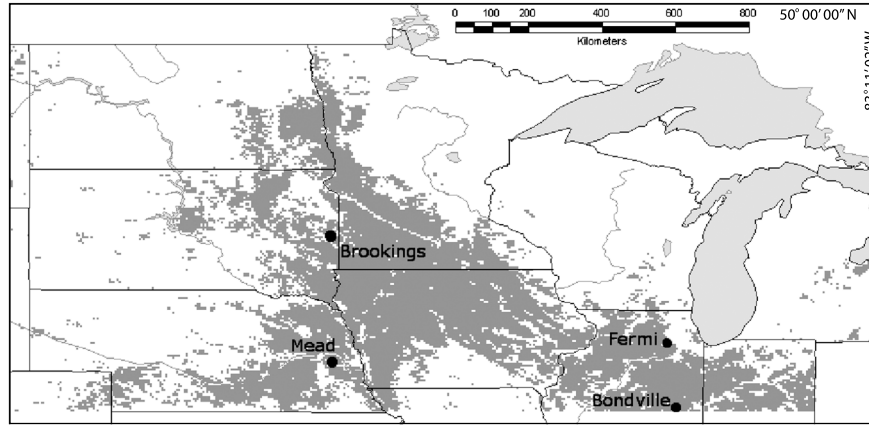
Figure 1. The study area (dark gray), Northern Great Plains, encompassing Nebraska, Iowa, Minnesota, North Dakota, and South Dakota, USA. The dark gray areas are defined by 0.05° grid cells with at least 50% MODIS mapped maize or soybean crop cover during 2007–2009 that are also labeled as cropland or grassland in the MODIS land cover product. The four dots show the locations of flux towers used for the EDPM training.

2.2.1. Model for Evapotranspiration Estimation

[8] The VegET model provides a simplified simulator of ET_a and, similar to *Godfrey et al.* [2007], *Kang et al.* [2009] and *Yuan et al.* [2010], relies on the Penman-Monteith equation to calculate daily reference evapotranspiration (ET_0). The daily ET_a is derived as the product of ET_0, K_s, and K_{cp} where K_s is the daily soil water stress parameterized from North American Land Data Assimilation System (NLDAS) soil water content data and K_{cp} is a canopy phenology coefficient derived from a 15 year climatology of satellite-derived NDVI [*Senay*, 2008]. Importantly, as vegetation phenology has interannual variability [*Pitman*, 2003], in this study, we derived K_{cp} values from EDPM-generated seasonal NDVI trajectories.

2.2.2. Model for Estimation of Canopy Phenology Coefficient

[9] The EDPM can simulate seasonal NDVI dynamics [*Kovalskyy and Henebry*, 2012a] using a similar set of forcings as the Penman-Monteith equation [*Monteith*, 1965]. The EDPM transforms continuous meteorological forcings into transient "events" that can potentially modify NDVI trajectories. From such events, the model predicts the seasonal NDVI trajectories at a daily temporal resolution. Currently, EDPM provides support for six kinds of forcings/events: (1) rain, (2) heat stress, (3) frost, (4) insufficient insolation, (5) excessive vapor pressure deficit, and (6) thermal time or growing degree-days. The model provides a computationally inexpensive replacement for a dynamic vegetation model, and it can work in both prognostic and diagnostic modes. In diagnostic mode, the EDPM corrects its predictions with satellite observations assimilated via a fast one-dimensional Kalman filter (1-DKF), which is especially advantageous for spatially explicit model applications [*Nagler et al.*, 2008; *Turner et al.*, 2008; *Campo et al.*, 2009; *Meng et al.*, 2009; *Anderson et al.*, 2011; *Miralles et al.*, 2010; *Godfrey and Stensrud*, 2010, *Lewis et al.*, 2012].

[10] Prior to this evaluation, the EDPM was successfully tested only in point-based experiments [*Kovalskyy and Henebry*, 2012a,2012b]. However, the spatially explicit application of the EDPM required amendments to the functioning of the EDPM phenological phase control module in order to match the variability of the growing season dates within a wider range of conditions. The existence of latitudinal gradients in phenology has long been recognized [*Hopkins*, 1918]. Vegetation phenology in the humid to subhumid extratropics responds primarily to temperature and daylength [*Running et al.*, 2004]. Daylength is a function of latitude, and temperature is strongly linked to insolation and thus daylength. We used the latitudinal patterns in the parameter coefficients from a simple quadratic model linking NDVI to thermal time [*de Beurs and Henebry*, 2004, 2005, 2010] to "transplant" the EDPM-derived start-of-season and growing season length using linear and inverse linear functions of latitude, respectively [*Henebry*, 2010].

2.2.3. The VegET and EDPM Coupling for the Evaluation

[11] Using the preplanned workflow (Figure 2), the coupled EDPM-VegET model was run in a prognostic mode and in a diagnostic mode. In prognostic mode, the EDPM used only meteorological data and linear mixing to produce seasonal NDVI trajectories for 0.05° grid cells in the study area. In diagnostic mode, the EDPM's prediction was corrected via a one-dimensional Kaman Filter (1-DKF) with MODIS NDVI observations defined as

$$\text{NDVI} = \frac{\rho_{\text{NIR}} - \rho_{\text{red}}}{(\rho_{\text{NIR}} + \rho_{\text{red}})} \qquad (1)$$

where ρ_{red} and ρ_{NIR} are the red and near-infrared reflectance. The EDPM also produced maps of phenological timing separately for maize, soybeans, and grassland.

[12] Daily EDPM NDVI was estimated prognostically in each 0.05° grid cell by modeling the mixed cropland covers as follows:
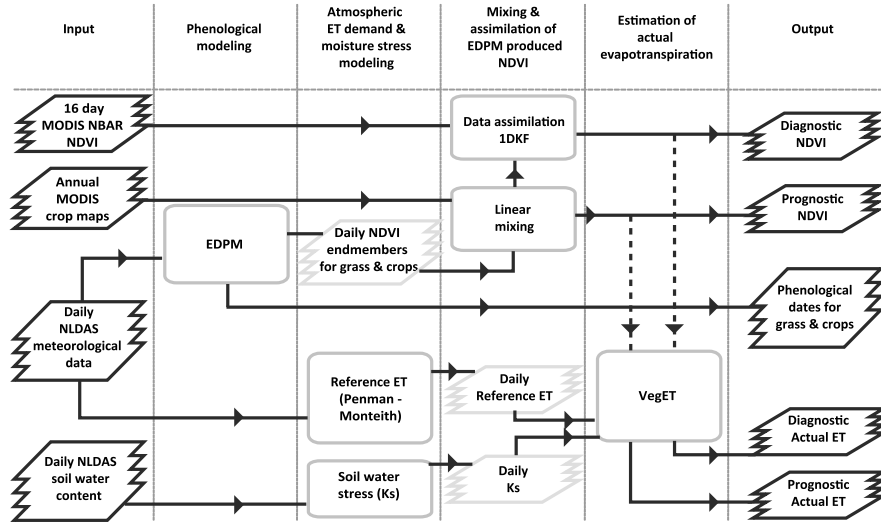
Figure 2. Modeling workflow. Rounded boxes are modeling and data preparation procedures; stacks are data time series.

$$\text{NDVI} = \sum_{i=1}^{3} f_i \ \text{NDVI}_i^{\text{endmember}} \qquad (2)$$

$$\sum_{i=1}^{3} f_i = 1$$

where f_i is the fraction (0–1) of the 0.05° grid cell that is cover type i ($i=1$: maize, $i=2$: soybean, $i=3$: grassland) and $\text{NDVI}_i^{\text{endmember}}$ is the EDPM-modeled NDVI value for that grid cell assuming 100% cover of cover type i. We note that direct linear mixing of NDVI values in this manner has been criticized in the literature since the NDVI is not a linear function of red and near infrared reflectance [*Settle and Campbell*, 1998; *Busetto et al.*, 2008]. However, we found that this had small impact for this study and that the error it creates is generally smaller than that due to MODIS reflectance errors propagated into the NDVI.

[13] The daily K_{cp} data were derived from the EDPM NDVI as follows:

$$K_{cp} = 1.22 \, \text{NDVI} + 0.01 \qquad (3)$$

where NDVI is the EDPM-derived NDVI defined as (2). The linear coefficients in (3) were derived by a statistical analysis of 8 years of flux tower ET_a and ET_0 measured at four flux towers (Figure 1) located in Mead, Nebraska (three towers) and Bondville, Illinois (one tower) and described in *Kovalskyy and Henebry* [2012b]. The four towers represent typical conditions for rain-fed commodity crops in the Central USA with maize-soybean rotation annually. The relationship (3) was derived by regression analysis with $n=842$, $r^2=0.46$ ($p<0.01$). Both the prognostic and diagnostic daily EDPM NDVI data were used in the VegET to produce corresponding prognostic and diagnostic ET_a results.

2.3. Model Parameterization Data

[14] The experiments conducted within this investigation used various data sources to reach its goals: (1) running the EDPM-VegET coupling scheme required meteorological forcing data; (2) percent crop cover data were necessary for the EDPM to produce seasonal canopy trajectories of model grid cells with mixed vegetation cover; (3) satellite NDVI data were used to assess the EDPM's predictions of seasonal canopy trajectories and later to produce retrospective outcomes.

2.3.1. Meteorological Forcings

[15] Meteorological forcings for the EDPM and the VegET were supplied by the North American Land Data Assimilation System in native General Regularly-distributed Information in Binary 1 format (1 h temporal and 0.125° grid cells). The original hourly data time series were aggregated into daily time series of 2 m air temperature (K) (daily average, maximum, and minimum); 2 m specific humidity (kg/kg) (daily average); surface pressure (Pa) (daily average); U wind component (m/s) (daily average); V wind component (m/s) (daily average); downward shortwave radiation (W/m^2) (daily sum); downward longwave radiation (W/m^2) (daily sum); total precipitation (mm) (daily sum), and soil water content at 1 m depth (kg/m^3) (daily average). The forcing data set and LSM simulations of NASA's Mosaic model from NLDAS Phase 2 were obtained from the NASA Goddard Earth Sciences Data and Information Services Center at http://disc.sci.gsfc.nasa.gov/hydrology/data-holdings.

2.3.2. Crop Cover Data

[16] This modeling experiment used annual 500 m crop cover maps for 2007, 2008, and 2009 derived via decision tree classification of the seven MODIS visible to shortwave infrared reflectance bands and derived temporal metrics that capture surface changes [*Chang et al.*, 2007]. As recommended in the original publication [*Chang et al.*, 2007], annual crop maps were mosaicked

from independently derived crop maps for Nebraska, Iowa, Minnesota, North Dakota, and South Dakota. The crop coverages in the mosaicked maps present the percentage of area under maize and soybean in each 500 m MODIS grid cell, provided that the grid cell has at least 50% of the area in either crop. The remaining proportion was assumed to be grassland, because grassland is the second most abundant land cover within the Northern Great Plains [*Luo et al*., 2003]. Additionally, MODIS 1 km land cover product [*Friedl et al*., 2002] (MCD12C1, International Geosphere–Biosphere Programme classification type available at ftp://e4ftl01.cr.usgs.gov/MOTA/MCD12C1.005) was used to insure that selected 500 m pixels are also labeled as grassland or cropland in the corresponding year.

2.3.3. Satellite NDVI Data

[17] Image time series of NDVI data were generated from the 0.05° MODIS nadir bidirectional reflectance distribution function (BRDF) adjusted reflectance (NBAR) product [*Schaaf et al*., 2002] (MCD43C4 version available at ftp://e4ftl01.cr.usgs.gov/MOTA/MCD43C4.005). The MODIS NBAR product is a 16 day product generated on a temporally overlapping basis every 8 days. The MODIS red and near-infrared NBAR were screened by examination of the associated product quality assessment bits to reject poor quality and snow contaminated retrievals and then used to generate NDVI as (1). The NDVI derived from the MODIS NBAR product has been shown to capture vegetation phenology [*Zhang et al*., 2006; 2009; *de Beurs et al*., 2009; *Kovalskyy et al*., 2011].

[18] These three data sets were reprojected as necessary into the geographic (latitude/longitude) MODIS climate modeling grid into 0.05° grid cells using the nearest neighbor resampling procedure to preserve the original data values. Resampled data were used to parameterize the coupled EDPM and VegET models in as illustrated in Figure 2.

2.4. Model Output Assessment Methodology and Validation Data

[19] We used three comparisons to assess model performance: (1) a comparison of the EDPM NDVI with the MODIS NDVI; (2) a comparison of the phenological dates produced by the EDPM with date from the NASS Crop Progress reports; and (3) a comparison of EDPM-VegET predictions of actual evapotranspiration with the evapotranspiration products from MODIS Land Suite and from the Mosaic model in NLDAS.

2.4.1. Assessment of NDVI Produced by the EDPM in Prognostic Mode

[20] The EDPM NDVI generated in prognostic mode were compared with NDVI calculated from the MODIS NBAR product. To match the nominal temporal date of the MODIS NDVI composites, only the EDPM NDVI values from the 8th day of the 16 day MODIS compositing period were compared. Because the EDPM cannot produce NDVI outside the growing season, the comparisons were restricted to the period early March to late October (day of year 97 to 305) for each of 2007, 2008, and 2009.

2.4.2. Assessment of Phenological Dates Estimated by the EDPM in Prognostic Mode

[21] The EDPM estimates of the start-of-season (SoS) and end-of-season (EoS) and length-of-season (LoS) were compared with U.S. National Agricultural Statistics Service (NASS) weekly reports (from http://www.nass.usda.gov/Charts_and_Maps/Crop_Progress_&_Condition/) on maize emergence and maturity respectively and with NASS weekly reports of soybean emergence and leaf-drop, respectively. The NASS data describe the county and state percentage crop area that underwent a given phenological phase transition for each calendar week but were only available for 2008 and 2009 across all the study area. Only the state level NASS data were used as some of the county level data were missing. For each state, the day when 50% of the crop was emergent was derived by linear interpolation of the dates of the two NASS reporting weeks with less than and more than 50% crop emergence. This NASS-derived state level crop emergence date was compared with the EDPM day that had 50% of 0.05° state grid cells labeled as SoS. Similarly, the interpolated state NASS days with 50% maize maturity and 50% soybean leaf-drop were compared with the EDPM day that had 50% of 0.05° state grid cells labeled as EoS for these crops. These dates were also derived for 25% and 75% values to capture state level temporal variability measured by interquartile range (IQR). The 50% LoS values from the NASS reports were calculated by subtracting the 50% SoS day of year from 50% EoS day of year. For the IQR LoS, the 75% LoS was calculated as 75% EoS date minus 25% SoS date, and the 25% LoS was computed as 25% EoS date minus 75% SoS date. The difference between 75% LoS and 25% LoS made the IQR of LoS from NASS reports. The IQR in the LoS estimated by the EDPM were collected directly from the model reports on the grid cell basis.

2.4.3. Assessment of Actual Evapotranspiration Estimated by the Coupled EDPM-VegET in Prognostic and Diagnostic Modes

[22] Prognostic and diagnostic daily ET_a estimates from the coupled EDPM-VegET model were compared with MODIS and Mosaic land surface model ET_a estimates. The 1 km 8 day MODIS evapotranspiration product (MOD16) presents estimates of 8 day sums of actual and reference ET modeled from weather forcings and remotely sensed land surface properties of the land surface [*Mu et al*. 2009]. Standard Hierarchical Data Format files were obtained from *ftp.ntsg.umt.edu/pub/MODIS/Mirror/MOD16/MOD16A2.105_MERRAGMAO/*. The MODIS ET product has been shown to match closely in situ ET_a measurements but has varying spatial and temporal uncertainties [*Mu et al*., 2009, 2011]. Therefore, we also used ET_a estimates defined from NASA's Mosaic LSM [*Koster and Suarez*, 2003; *Koster et al*., 2004]. Similar to MOD16 product, NASA's Mosaic LSM has shown differential spatial and temporal performance during validation experiments [*Xia et al*., 2012a, 2012b]. The Mosaic ET_a data are defined hourly in 0.125° grid cells and were aggregated into daily estimates by summation. The coupled model and Mosaic estimates were summed into 8 day totals so that they could be compared with
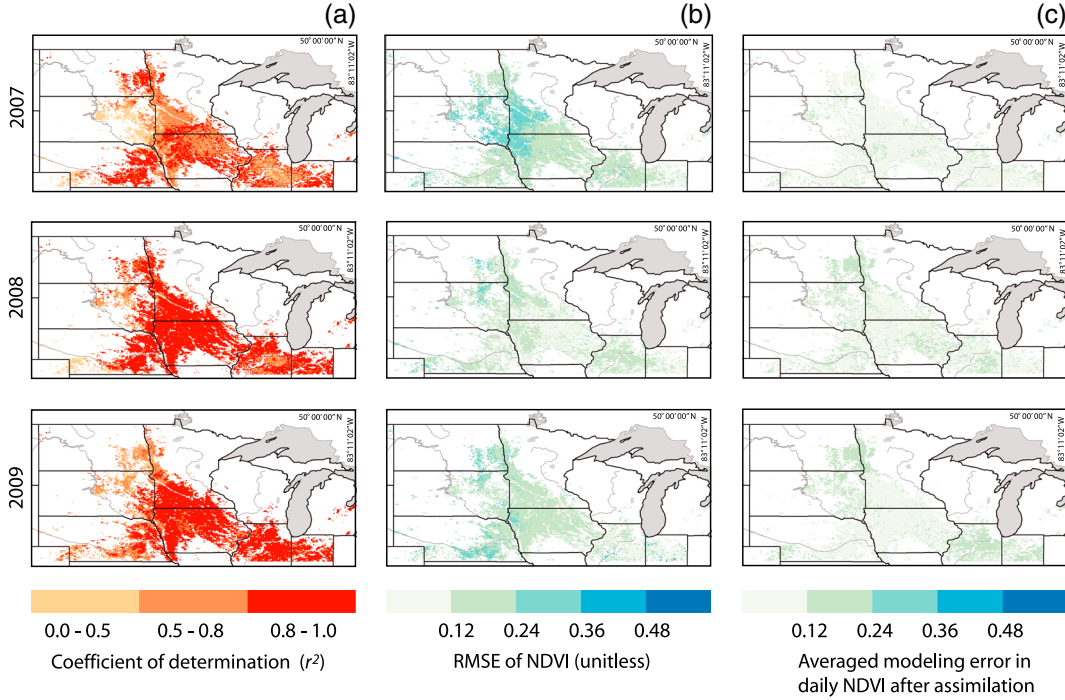
Figure 3. Comparison of the EDPM NDVI against MODIS NDVI within the study area. (a) Coefficient of determination (r^2); (b) root mean square error NDVI; (c) seasonally averaged daily NDVI error after assimilation of MODIS NDVI observations.

the 8 day MODIS ET_a product. As with the evaluation of NDVI, only within growing season ET_a results were considered for 2007, 2008, and 2009.

[23] In the above NDVI and ET_a assessments, the two most common measures of performance: coefficient of determination (r^2) and root mean square error (RMSE) were derived as below:

$$r^2 = 1 - \frac{\sum (m - c)^2}{\sum (c - \bar{c})^2} \qquad (4)$$

$$\text{RMSE} = \sqrt{\frac{\sum (m - c)^2}{n}} \qquad (5)$$

where m is the modeled NDVI or ET_a, c is the comparison reference NDVI or ET_a, and n is the total number of modeled and reference values. Along with r^2 and RMSE, we examined the spatiotemporal patterns of residuals ($m - c$) to identify conditions where coupled scheme maintains or loses its adequacy. Previous testing of the EDPM and VegET at flux tower locations showed high levels of performance for the coupled model [*Kovalskyy and Henebry*, 2012a, 2012b]. In this regional application of the coupled model, the performance expectations are given by the earlier point-based performances; namely, for NDVI estimates, $r^2 = 0.8 \pm 0.1$ with RMSE = 0.1 ± 0.025, and for ET_a, $r^2 = 0.7 \pm 0.15$ with RMSE = 1.4 ± 0.5 mm per day, and transforming into 8 day aggregates by simple multiplication yields RMSE = 11.2 ± 4 mm per 8 days.

3. Results

3.1. Comparison of the EDPM-derived NDVI With MODIS NDVI

3.1.1. Spatial Comparison of the EDPM NDVI Against MODIS NDVI

[24] The maps representing performance measures for each year show that the performance of the EDPM-generated NDVI varies across the study area (Figure 3). We also included the maps of average seasonal modeling errors (Figure 3c) from results received after the data assimilation (diagnostic mode) to contrast those with RMSE obtained during uncorrected (prognostic) estimation.

[25] The r^2 maps in left column (Figure 3a) clearly demonstrate that the EDPM NDVI time series well correlate with observed dynamics of MODIS NDVI. The r^2 maps are dominated by dark color representing coefficients of determination of 0.8 and greater (Figure 3a). The coefficients of determination had a tendency to decrease toward the western edge of the study area, showing the worst performance in 2007 and best in 2008 with mean r^2 of 0.77 and 0.86, respectively. This assessment is supported by the RMSE maps (Figure 3b): the overall RMSE across the study area reached 0.18 in 2007 but dropped to just above 0.11 for 2008. Unlike with prognostic mode of the EDPM, the maps produced in diagnostic mode (Figure 3c) show the even spatial distribution of average modeling errors after the EDPM NDVI has assimilated the MODIS NDVI observations. The magnitudes of modeling errors with assimilated NDVI were slightly less than 0.1 and similar in all 3 years.
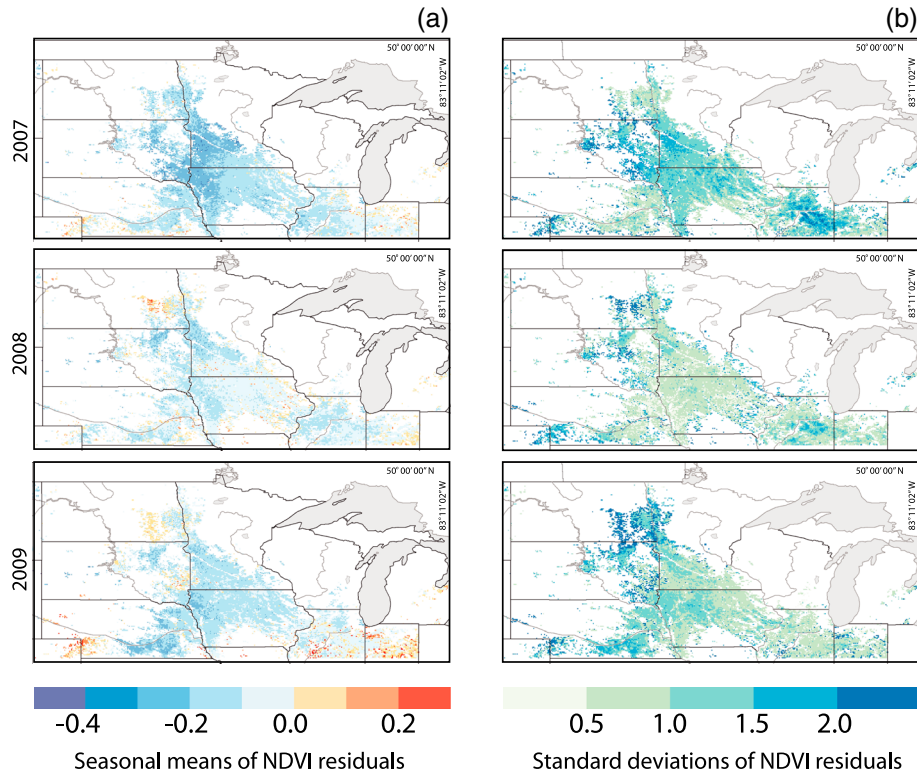
Figure 4. Spatial distributions of residuals ($NDVI_{EDPM} - NDVI_{MODIS}$): (a) Seasonal means of NDVI residuals and (b) standard deviations of NDVI residuals.

[26] Compared to MODIS NDVI observation, the EDPM NDVI was mostly lower in the central part of the study area and higher at the periphery (Figure 4). The 2007 results came out as the most biased having the mean of residuals -0.2 to -0.3 spread along the western Iowa and Minnesota borders. For 2008 and 2009, most of the seasonally averaged differences between observed and modeled NDVI varied between -0.2 and 0.1. The variability of the residuals grew from the center toward the periphery (Figure 4b). Importantly, similar absolute values of RMSE (Figure 3b) and mean residuals (Figure 4a) point that the bias was rather uniform for most of the study area.

3.1.2. Temporal Comparison of the EDPM NDVI Against MODIS NDVI

[27] A closer look into seasonal dynamics of residuals (Figure 5) reveals similarities in developments seen in both the mean difference from observations and the standard deviation of residuals within the three growing seasons.

[28] Comparable seasonal patterns of residuals are evident and similar in 3 years (Figure 5). The graphs show that the EDPM prediction of NDVI was only slightly lower than MODIS observations early in the year when grasses enter their growing phase, but later the underestimation increased substantially as the growing season commenced for maize and soybeans. The means of residuals became more negative at the approach of each phenophase transition, which has been previously identified as a source of error in the EDPM [*Kovalskyy and*

Henebry, 2012a,b]. After the change of phenophase, differences with observations returned to the initial level. Overall, the analysis of the EDPM performance suggests that although the errors from EDPM were higher, they were still within the expected range based on prior performance validation [*Kovalskyy and Henebry*, 2012a].
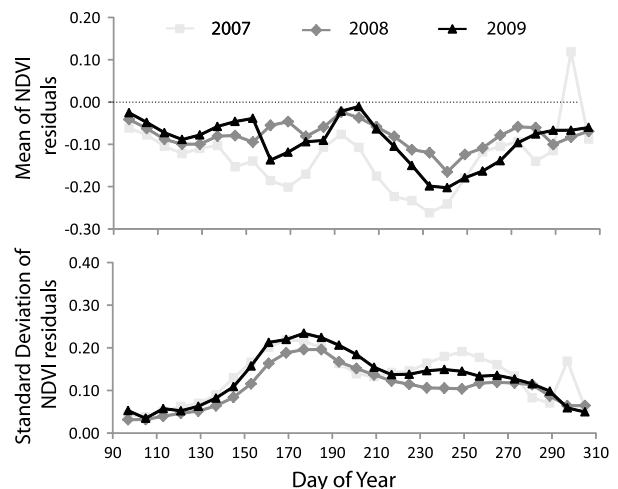

Figure 5. Temporal dynamics of residuals ($NDVI_{EDPM} - NDVI_{MODIS}$) during three growing seasons. Light grey squares represent 2007; darker grey diamonds are 2008; and black triangles are 2009.
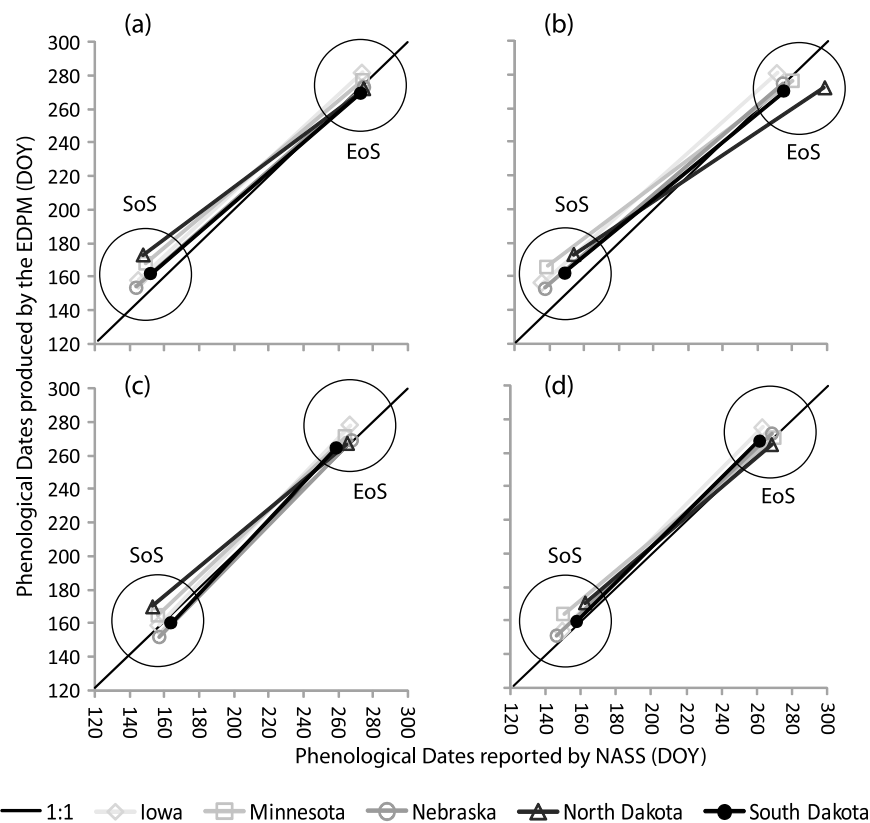
Figure 6. Contrasted start and end dates of the growing season for the two crops and 2 years estimated by the EDPM and reported by NASS recounted in days of year. Circles signed SoS and EoS denote start-of-season and end-of-season, respectively. (a) SoS and EoS for maize in 2008, (b) SoS and EoS for maize in 2009, (c) SoS and EoS for soybean in 2008, and (d) SoS and EoS for soybean in 2009.

3.2. Comparison of Growing Season Dates

[29] Here we highlight the differences between the SoS and EoS dates estimated by EDPM and those reported by NASS.

[30] Fairly good agreement is evident between observed and estimated SoS and EoS dates of the two growing seasons (Figure 6). Persistent delays of about 2 weeks in SoS for maize crops within all five states are also apparent (Figure 6). Such delays in SoS predictions were comparable with the mismatches encountered in retrospective NDVI analyses by *Fisher et al.* [2006], *Zhang et al.* [2009], and *Kovalskyy et al.* [2011]. Meanwhile, the estimates of both SoS and EoS for soybeans were more accurate and consistent. Length-of-season (LoS) for NASS data show higher degree of variability than EDPM estimated ones (Figure 7); similar patterns occur in the variability of SoS and EoS (data not shown).

3.3. Comparison of Et$_a$ Estimated with the EDPM-VegET with the MODIS and Mosaic Et$_a$ Products

3.3.1. Temporal Comparison of the EDPM-VegET Produced Et$_a$ Against Reference Data Sets

[31] Before comparing the ET$_a$ estimates from the coupled EDPM-VegET with references, it is important to note the substantial discrepancies between the two reference data sets (Figure 8a). The plot clearly shows that,
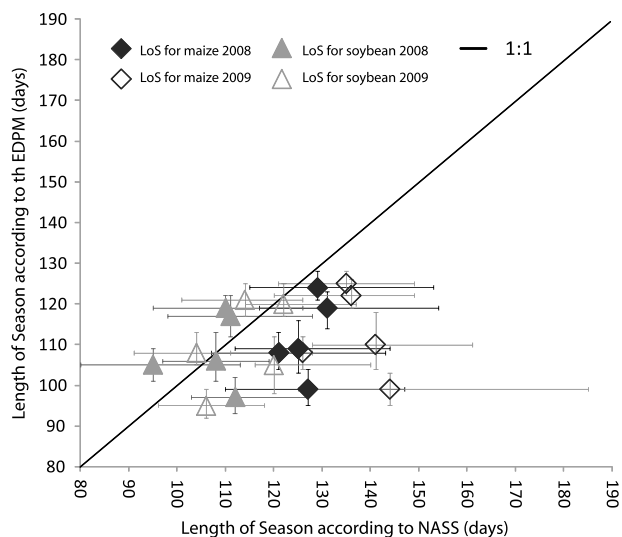

Figure 7. Contrasts between the EDPM estimates and NASS reports of the length-of-season and its variability for the two crops and 2 years. Symbols show the average and error bars display the interquartile range (IQR). Filled diamonds show LoS for maize in 2008, open diamonds show LoS for maize 2009, filled triangles show LoS for soybean 2008, and open triangles show LoS for soybean 2009.
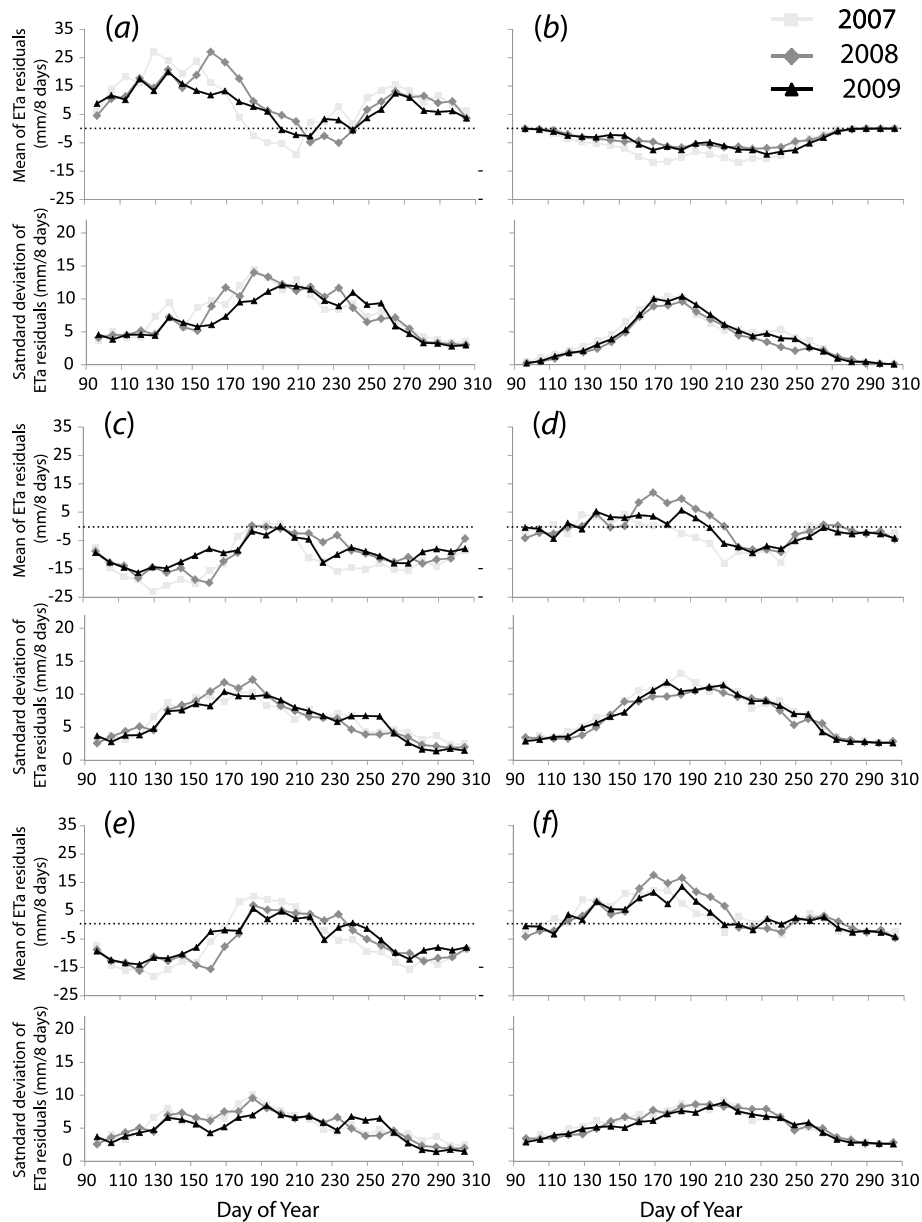
Figure 8. Temporal dynamics of ET_a residuals during the 2007–2009 growing seasons. (a) $ET_{a\ Mosaic}$ $ET_{a\ MOD16}$; (b) $ET_{a\ EDPM\text{-}VegET} - ET_{a\ EDPM\ with\ 1\text{-}DKF\text{-}VegET}$; (c) $ET_{a\ EDPM\text{-}VegET} - ET_{a\ Mosaic}$; (d) $ET_{a\ EDPM\text{-}VegET} - ET_{a\ MOD16}$; (e) $ET_{a\ EDPM\ with\ 1\text{-}DKF\text{-}VegET} - ET_{a\ Mosaic}$; (f) $ET_{a\ EDPM\ with\ 1\text{-}DKF\text{-}VegET} - ET_{a\ MOD16}$. Light grey squares represent season of 2007, darker grey diamonds are 2008, and black triangles are 2009.

compared with MOD16 product, Mosaic ET_a first was higher and then came close to zero difference by the middle of the growing season. Later, however, the Mosaic ET_a turned to overestimation again. In contrast, the differences between the two versions of the EDPM-VegET estimates representing ET_a derived with and without assimilation via 1-DKF scheme were apparent only in the middle of the growing season (Figure 8b). The ET_a prediction by coupled model was following the previously noted underestimation pattern in NDVI produced by the EDPM in prognostic mode (Figure 5). Hence, the prognostic ET_a values were lower than ET_a produced in diagnostic mode (with 1-DKF). The variability of residuals exhibited

similar temporal behavior to the one found earlier (compare Figure 8b with Figure 5). The remaining subpanels (Figures 8c–8f) retain the main features evident in subpanels of Figures 8a and 8b.

[32] The subpanel (Figure 8c) reveals that at the beginning of growing season, prognostic EDPM-VegET results showed underestimation of 15 mm per 8 days compared to ET_a produced by Mosaic. In the midseason, the difference came close to zero, but later a smaller (~10 mm per 8 days) underestimation prevailed again (Figure 8c). Compared to the ET_a from MOD16, the predictions from the EDPM-VegET showed close to zero difference for most of the season with slight overestimation in early June (up to
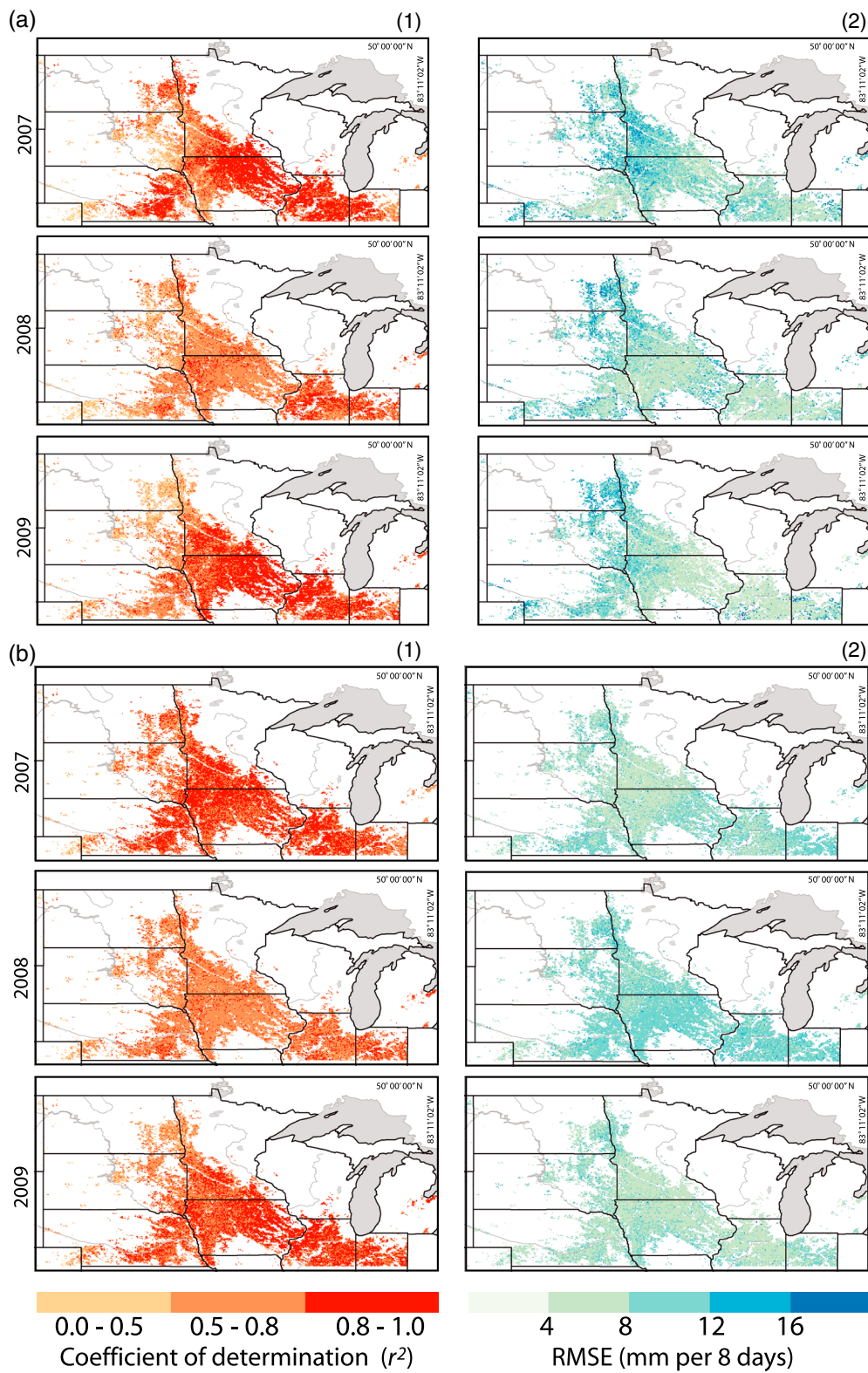
Figure 9. Comparison of MOD16 ET_a with the ET_a produced by EDPM-VegET working in (a) prognostic mode and (b) diagnostic mode involving 1-DKF assimilation. (1) Coefficient of determination (r^2); (2) root mean square error (mm per 8 days).

Figure 10. Spatial distributions of residuals (a) $ET_{a\ EDPM-VegET} - ET_{a\ MOD16}$ (b) $ET_{a\ EDPM\ with\ 1-DKF-VegET} - ET_{a\ MOD16}$. (1) Seasonal mean of residuals (mm per 8 days); (2) standard deviation of residuals (mm per 8 days).

7 mm per 8 days) and underestimation of the same magnitude in late August (Figure 8d). The variability of residuals for prognostic ET_a estimates remained high and had a clear seasonal pattern.

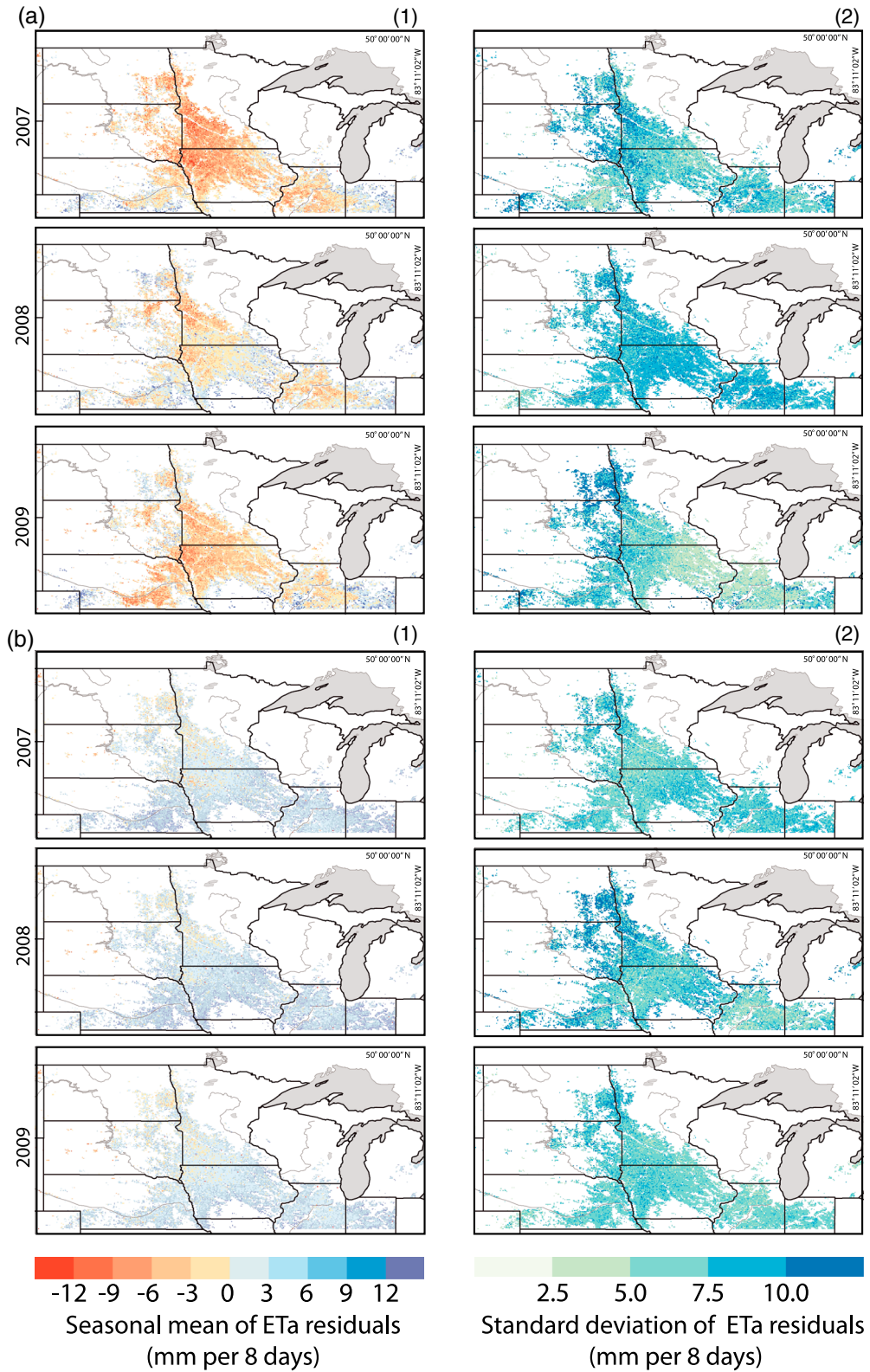[33] Differences between reference data and estimates of ET_a obtained with the EDPM-VegET working in diagnostic mode (with 1-DKF) exhibited temporal patterns seen previously in prognostic results. Differences with Mosaic ET_a were negative at the beginnings of growing seasons (Figure 8e), but in the midseason, the curves drifted toward slight (up 5 mm per 8 days) overestimation but later reverted to underestimation of 15 mm per 8 days (Figure 8e). Compared with MOD16 ET product, the EDPM-VegET diagnostic estimates produced residuals that signal slight overestimation early in the growing season. Later, however, the residuals came close to zero and remained there till the end of growing season indicating good match (Figure 8f). The variability of residuals for diagnostic ET_a estimates from EDPM-VegET dropped quite dramatically in both comparisons (Figures 8e and 8f) showing the relative efficacy of data assimilation for this method of ET_a estimation.

3.3.2. Spatial Comparison of the EDPM-VegET Produced Et_a Against Reference Data Sets

[34] The comparison with MOD16 product demonstrated that the EDPM-VegET scheme was able to follow the dynamics of ET_a in the reference data set and produced high coefficients of determination, even exceeding the expectations of 0.7 ± 0.15 (Figures 9a and 9b). Average coefficient of determination was more than 0.8 for both prognostic and diagnostic modes. In 2008, the average r^2 dropped to the expected 0.7 level for both versions of derived ET_a (Figures 9a and 9b). Compared to the coefficients of determination in Figure 9a1, the distribution of r^2 values within the study area was more homogeneous in the results from the coupled scheme working in diagnostic mode involving 1-DKF assimilation with MODIS NDVI data (Figure 9b1). In both modes, the EDPM-VegET scheme showed lower r^2 in the western peripheral regions where the accuracy of crop cover maps was known to be lower. RMSE values in those regions were correspondingly higher especially in the results of the scheme working in prognostic mode. In diagnostic mode, RMSE had a more uniform distribution and constituted around 6 mm per 8 days on average, which is half of the expected level of 11.2 mm per 8 days. The average RMSE for EDPM-VegET outcomes derived in prognostic mode was about 8 mm per 8 days. Transformed into corresponding units, this performance would be comparable to *Nagler et al.* [2005] or *Abramowitz et al.* [2008], if the ET_a data from MOD16 product approximated the reality with the accuracy of flux tower instruments [*Mu et al.*, 2009]. A point-based flux tower validation study has shown that the scheme can approximate daily ET_a in crops with similar accuracy [*Kovalskyy and Henebry*, 2012b].

[35] The contrast between the two sets of ET_a estimates from the EDPM-VegET scheme is readily apparent in the maps of mean seasonal residuals (Figures 10a1 and 10b1). In prognostic mode (Figure 10a), the prediction of ET_a had mostly negative mean residuals changing to positive in the periphery of the study region (both east and west). Predominantly, mean seasonal residual values (Figure 10a1) deviated not too far from zero with worst cases of -12 mm per 8 days in 2007 in the central part of the study region. Standard deviations of ET residuals (Figure 10a2) shows uneven distribution of variability revealing clusters of unstable performance from EDPM-VegET scheme working in prognostic mode. Meanwhile, the performance of the EDPM-VegET scheme was more stable in diagnostic mode (Figure 10b). The mean residuals in the left column (Figure 10b1) were mostly positive, fluctuating no more than 9 mm per 8 days. There was less contrast between years and also less heterogeneity within the study region. Smaller and more homogenously distributed standard deviations of residuals (Figure 10b2) indicated more spatially stable performance in diagnostic mode compared to prognostic mode (Figure 10a2).

[36] Overall, the EDPM-VegET scheme showed closer temporal and spatial correspondence with MOD16 product but contrasted with the ET_a estimates from the Mosaic estimates (section A); the results from the EDPM-VegET scheme were less correlated and had greater spatial variability in RMSE and residuals. Figures in section A demonstrate the problem in the central part of the study area (especially during 2007 growing season) that came from numerous differences in approaches to the ET_a modeling and in assumptions made about the parameterization data, e.g., land cover types, soil types, and leaf area index [*Koster and Suarez*, 1996; *Mitchell et al.*, 2004]. Nevertheless, the expected performance of $r^2 = 0.7 \pm 0.15$ and RMSE $= 11.2 \pm 4$ mm per 8 days were achieved by the coupled models working only in diagnostic mode using MODIS observations for correction of simulated NDVI trajectories.

4. Discussion

[37] The overall impression from the comparisons is favorable in support of the EDPM-VegET coupling scheme. The results matched and even exceeded most of the expected measures of model performance obtained from point-based validations [*Kovalskyy and Henebry*, 2012a,2012b]. Based on comparison with MODIS NDVI observations, the EDPM NDVI trajectories may be useful in various applications, such as daily vegetation monitoring or phenological simulations with induced crop cover changes. For the latter, the EDPM will be particularly advantageous considering its simple assumptions and possibility of using mixtures of crops in grid cells. The coupled scheme has also produced ET_a results similar to those from the MODIS evapotranspiration product. Even in the worst cases, the RMSE measures in ET_a (10–14 mm per 8 days) were also comparable with those of *Senay* [2008], *Mu et al.* [2007], and *Abramowitz et al.* [2008]. It is possible, however, that the vegetation and hence the canopy phenology coefficient derived from the EDPM NDVI had a limited impact on the ET_a results from VegET driven mostly by meteorological forcings. Additionally, the performance of the EDPM VegET scheme may be affected by the choice of soil moisture data from Mosaic LSM that may carry errors from original vegetation representation. The impact of this issue on estimated ET_a requires further investigation on a daily basis.

[38] Further, the comparison between the MODIS NDVI and the NDVI produced by the EDPM revealed both temporal and spatial drawbacks in the performance of the event-driven model. The EDPM NDVI predictions for 2007 during late season drought produced higher residuals and RMSE compared to other years. The most likely reason for this performance drawback is the over-reaction of the EDPM to the 2007 drought (residuals dropped to -0.25) and the current inability of the model to account for irrigation. An appropriate solution for the 2007 error spike would be additional training of the EDPM on irrigated flux tower sites during the drought years so that the model can respond to hydrological stress more adequately within irrigated areas. During other years, the bias appeared to be consistent throughout the area and could be arithmetically removed from the results or corrected by obtaining better estimates of background vegetation-free NDVI values as suggested by *Zhang et al.* [2003]. Unlike spatial bias, the patterns seen in temporal dynamics of errors constitute a problem that cannot be corrected with an arithmetical transformation. Temporal spikes in residuals were related solely to the performance of automatic estimation of growing season dates in the EDPM. Therefore, the solution should come from improvements in functioning of the phenological control mechanism in the event-driven model.

[39] The variability and some mismatches of key growing season dates also became problematic for the EDPM. The contrast in IQR between LoS reported by the NASS and estimated by EDPM was expected since the spatial variability in LoS is driven by gradients in precipitation, temperatures, and daylength, [*Henebry*, 2010; *Ibanez et al.*, 2010]; however, the EDPM does not include precipitation as a phenological control at this stage [*Kovalskyy and Henebry*, 2012a]. Despite this shortcoming, the EDPM estimates of phenological dates for all crops and years managed to stay within the range of state-level reports from the NASS. The risk remains that these phenological mismatches may propagate into NDVI trajectories precluding further analysis based on uncorrected (prognostic) daily NDVI time series. Evidently, both NDVI and ET_a predictions from EDPM-VegET scheme exhibited increased error at times of phenophase transition. Meanwhile, the 1-DKF-corrected NDVI time series were less influenced by the errors in phenological timing, but diagnostic ET_a results were still higher then references early in the growing season. This overestimation indicates that, while decreasing the residuals and their variability, the assimilation of MODIS NDVI could not completely ameliorate the shortcomings of the EDPM-VegET scheme.

[40] Next steps for model improvement include attempts to eliminate the delays in SoS in maize by collecting new phenological data from flux towers or specialized phenological sites. The new data will allow refinement of the temperature, insolation, and calendar time triggers for phenological transitions in the EDPM. Also, we intend to improve the matching between the interannual variability in phenological dates from the EDPM and in NASS reports through inclusion of precipitation in the phenophase control mechanism. Special attention will be paid to the periphery of the study region, as those areas are most likely to carry land cover mapping errors: crop cover classification models were trained on representative areas located in the middle of cropland regions of the five states [*Chang et al.*, 2007].

5. Conclusion

[41] The purpose of the experiment described in this paper was to assess the fitness of the EDPM-VegET coupling scheme for spatially explicit application in a phenological modeling study within agricultural areas of Northern Great Plains. The study has helped to prioritize directions for model improvement so that future research can provide insights into how ET_a may change in response to changes in crop area and how potential future landscapes of rainfed croplands may affect regional hydrometeorology. Performance of the scheme was assessed through comparison of modeled variables with independent reference data sets. First, the EDPM-produced seasonal NDVI trajectories were found comparable with MODIS NDVI giving coefficients of determination of 0.65–0.95 and RMSE of 0.1 ± 0.035 for the entire study area. Assimilated MODIS NDVI brought the variability in modeling errors closer to the 0.1 NDVI level. Growing season dates estimated by the EDPM were matching the NASS reports, with less than 2 weeks of difference in key phenological dates in both maize and soybean crops. Estimates of actual evapotranspiration produced by the coupled scheme were compared with ET_a from Mosaic model and with the MODIS evapotranspiration product. In both comparisons, the performance targets of $r^2 = 0.7 \pm 0.15$ and RMSE $= 1.4 \pm 0.5$ mm per day were both met by the coupling scheme working in diagnostic mode using MODIS observations for correcting seasonal trajectories of canopy development. Overall, in every comparison, the EDPM-VegET coupling scheme proved its ability to model daily NDVI and ET_a dynamics that closely follow best available reference data.

[42] Minor issues of model performance were encountered during this experiment. The EDPM NDVI trajectories were biased toward underestimation relative to the MODIS NDVI reference; the bias was relatively uniform in space but less stable in time. Actual ET estimates from the EDPM-VegET were closer to MOD16 product, while producing greater differences with Mosaic LSM predictions. Spatial patterns in differences could be attributed to distinct assumptions about land cover in Mosaic LSM [*Mitchell et al.*, 2004]. Seasonal profiles of differences between EDPM-VegET estimates and reference data exhibited clear patterns driven by phenology. The impacts of these issues on performances of the EDPM and the VegET models, however, were relatively small and easily correctable. The EDPM-VegET coupling scheme has demonstrated its ability to reproduce both the spatial and temporal dimensions of NDVI and ETa dynamics within an acceptable range of error; therefore, the coupled model is recommended for use in spatially explicit applications and modeling studies in the humid to subhumid extratropics.
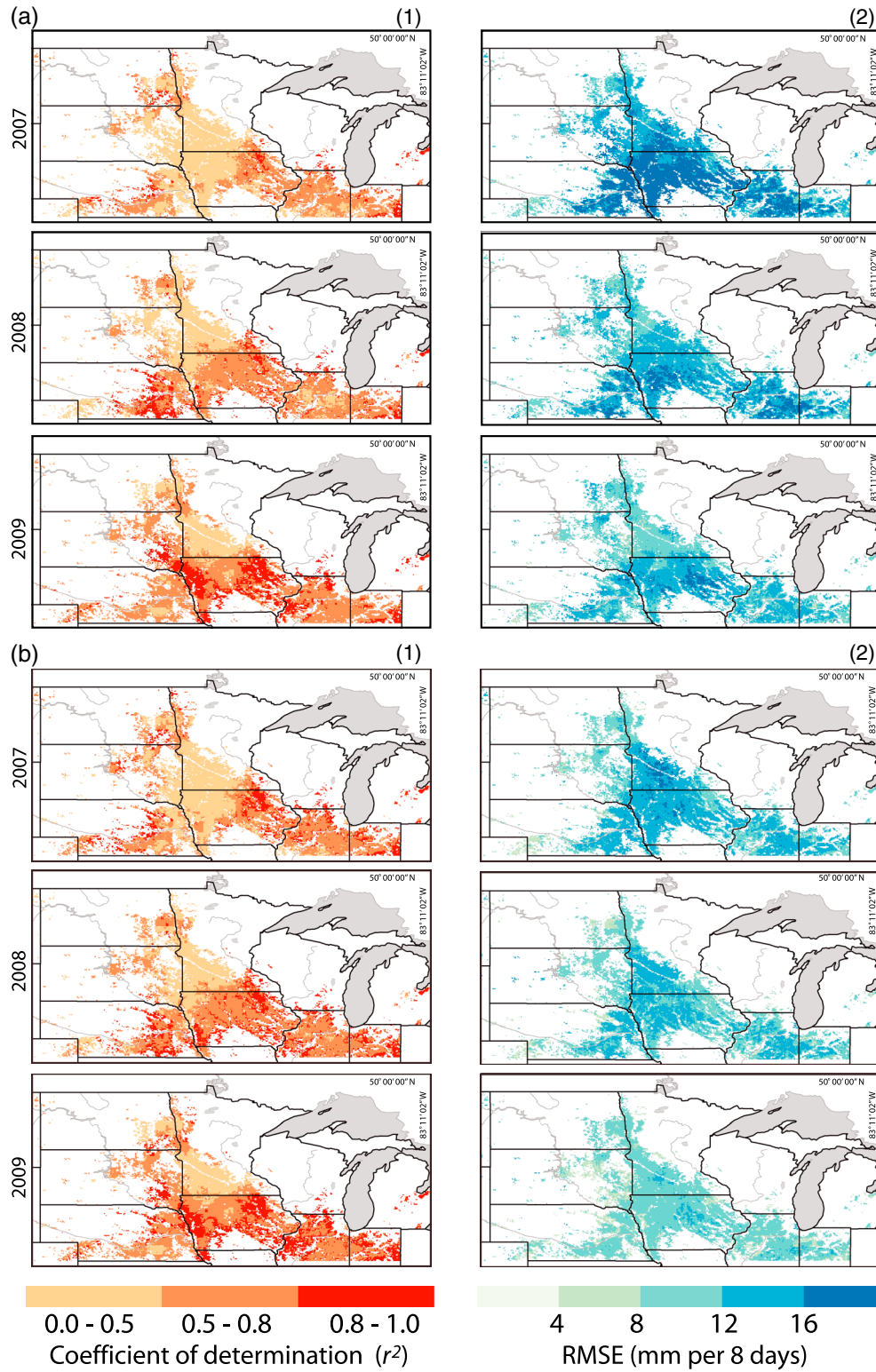
Appendix A

Figure A1. Comparison of ET_a from Mosaic LSM with the ET_a produced by EDPM-VegET from the review version coupling scheme deployed in (a) prognostic mode and (b) diagnostic mode involving 1DKF from the review version assimilation. (1) Coefficients of determination (r^2); and (2) Root mean square error (mm per 8 days).

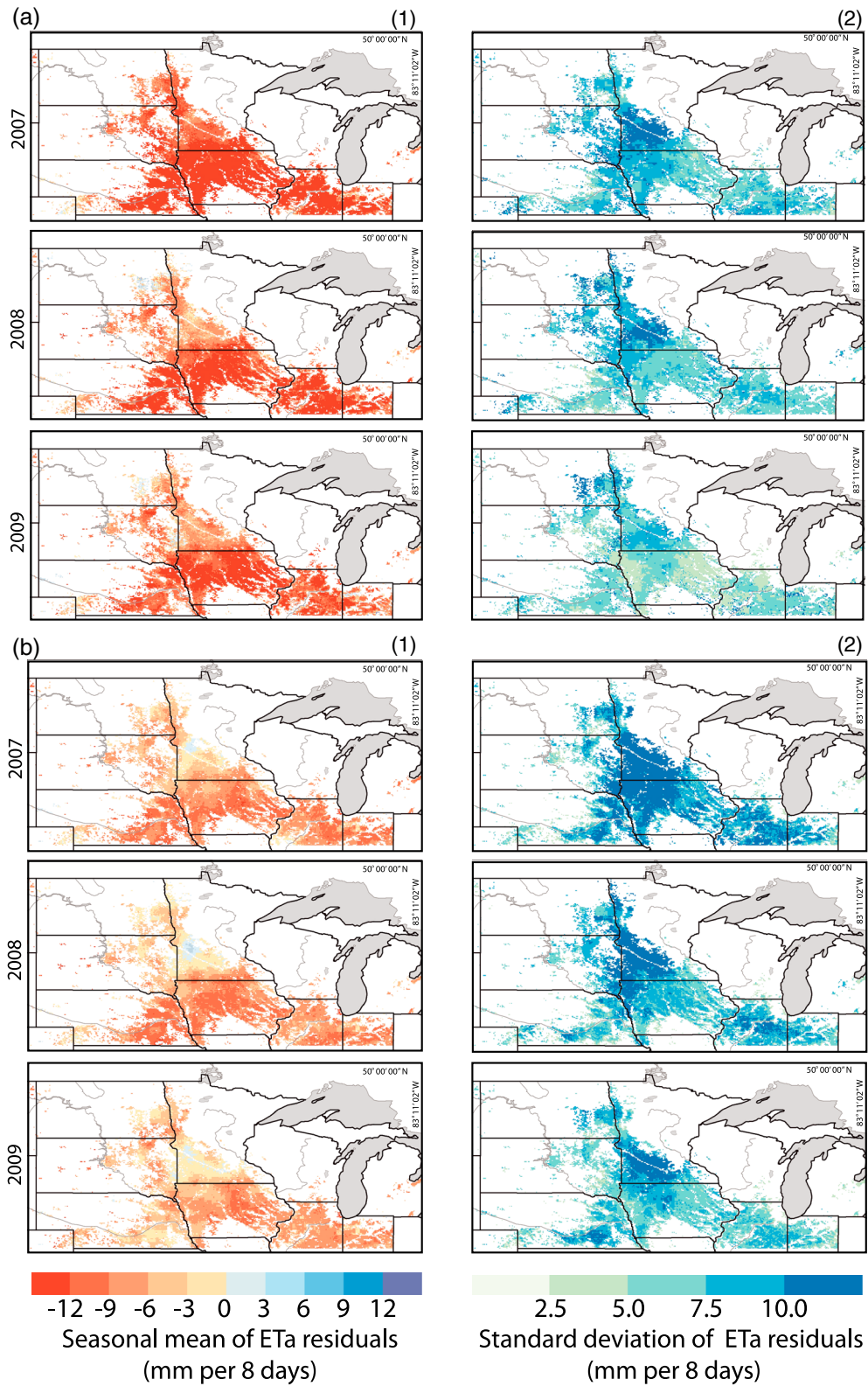**Figure A2.** Spatial distributions of residuals (a) $ET_{a\ EDPM\text{-}VegET} - ET_{a\ Mosaic}$ (b)$ET_{a\ EDPM\ with\ 1DKF} -$ from the review version $VegET - ET_{a\ Mosaic.}$ (1) Seasonal means of residuals (mm per 8 days); and (2) Standard deviations from the review version of residuals (mm per 8 days).

References

Abramowitz, G., R. Leuning, M. Clark, and A. Pitman (2008), Evaluating the performance of land surface models, *J. Clim.*, *21*(21), 5468–5481, doi:10.1175/2008JCLI2378.1.

Anderson, M. C., et al. (2011), Mapping daily evapotranspiration at field to continental scales using geostationary and polar orbiting satellite imagery, *Hydrol. Earth Syst. Sci.*, *15*(1), 223–239, doi:10.5194/hess-15-223-2011.

Busetto, L., M. Meroni, and R. Colombo (2008), Combining medium and coarse spatial resolution satellite data to improve the estimation of sub-pixel NDVI time series, *Remote Sens. Environ.*, *112*(1), 118–131, doi:10.1016/j.rse.2007.04.004.

Campo, L., F. Castelli, D. Entekhabi, and F. Caparrini (2009), Land-atmosphere interactions in a high resolution atmospheric simulation coupled with a surface data assimilation scheme, *Nat. Hazard. Earth Syst. Sci.*, *9*(5), 1613–1624, doi:10.5194/nhess-9-1613-2009.

Chang, J., M. C. Hansen, K. Pittman, M. Carroll, and C. DiMiceli (2007), Corn and soybean mapping in the United States using MODIS time-series data sets, *Agron. J.*, *99*(6), 1654–1664, doi:10.2134/agronj2007.0170.

Debaeke, P., J. P. Caussanel, J. R. Kiniry, B. Kafiz, and G. Mondragon (1997), Modelling crop: Weed interactions in wheat with ALMANAC, *Weed Res.*, *37*(5), 325–341, doi:10.1046/j.1365-3180.1997.d01-55.X.

de Beurs, K. M., and G. M. Henebry (2004), Land surface phenology, climatic variation, and institutional change: Analyzing agricultural land cover change in Kazakhstan, *Remote Sens. Environ.*, *89*, 497–509, doi:10.1016/j.rse.2003.11.006.

de Beurs, K. M., and G. M. Henebry (2005), A statistical framework for the analysis of long image time series, *Int. J. Remote Sens.*, *26*(8), 1551–1573, doi:10.1080/01431160512331326657.

de Beurs, K. M., and G. M. Henebry (2010), Spatio-temporal statistical methods for modelling land surface phenology, in *Phenological Research*, edited by I. L. Hudson and M. R. Keatley, pp. 177–208, Springer, Netherlands.

de Beurs, K. M., C. K. Wright, and G. M. Henebry (2009), Dual scale trend analysis for evaluating climatic and anthropogenic effects on the vegetated land surface in Russia and Kazakhstan, *Environ. Res. Lett.*, *4*, 045012, doi:10.1088/1748-9326/4/4/045012.

Dickinson, R. E., M. Shaikh, R. Bryant, and L. Graumlich (1998), Interactive canopies for a climate model, *J. Clim.*, *11*(11), 2823–2836, doi:10.1175/1520-0442(1998)011<2823:ICFACM>2.0.CO;2.

Fisher, J. I., J. F. Mustard, and M. A. Vadeboncoeur (2006), Green leaf phenology at Landsat resolution: Scaling from the field to the satellite, *Remote Sens. Environ.*, *100*(2), 265–279, doi:10.1016/j.rse.2005.10.022.

Foley, J. A., S. Levis, M. H. Costa, W. Cramer, and D. Pollard (2000), Incorporating dynamic vegetation cover within global climate models, *Ecol. Appl.*, *10*(6), 1620–1632, doi:10.1890/1051-0761(2000)010[1620: IDVCWG]2.0.CO;2.

Friedl, M. A., et al. (2002), Global land cover mapping from MODIS: Algorithms and early results, *Remote Sens. Environ.*, *83*(1–2), 287–302, doi:10.1016/S0034-4257(02)00078-0.

Gao, Z. Q., C. S. Liu, W. Gao, and N. B. Chang (2010), A coupled remote sensing and the Surface Energy Balance with Topography Algorithm (SEBTA) to estimate actual evapotranspiration under complex terrain, *Hydrol. Earth Syst. Sci. Discuss.*, *7*(4), 4875–4924, doi:10.5194/hessd-7-4875-2010.

Godfrey, C. M., and D. J. Stensrud (2010), An empirical latent heat flux parameterization for the Noah land surface model, *J. Appl. Meteorol. Climatol.*, *49*(8), 1696–1713, doi:10.1175/2010JAMC2180.1.

Godfrey, C., D. Stensrud, and L. Leslie (2007), A new latent heat flux parameterization for land surface models, paper presented at Preprints of 21st Conference on Hydrology, American Meteorological Society, San Antonio, TX, Jan15-18, 2007.

Henebry, G. M. (2010), Land surface phenology as an integrative diagnostic for landscape modeling, paper presented at LANDMOD2010, Montpellier, France, http://www.symposcience.org/exl-doc/colloque/ART-00002394.pdf.

Hopkins, A. D. (1918), Periodical events and natural law as guides to agri-cultural research and practice, in *Monthly Weather Review Supplement*, edited, Government Printing Office, Washington, DC.

Ibanez, I., R. B. Primack, A. J. Miller-Rushing, E. Ellwood, H. Higuchi, S. D. Lee, H. Kobori, and J. A. Silander (2010), Forecasting phenology under global warming, *Philos. Trans. R. Soc. B: Biol. Sci.*, *365*(1555), 3247–3260, doi:10.1098/rstb.2010.0120.

Iglesias, A., J. Schlickenrieder, D. Pereira, and A. Diz (2011), From the farmer to global food production: use of crop models for climate change impact assessment, in *Handbook on Climate Change and Agriculture*, edited by R. O. Mendelsohn and A. Dinar, p. 49, Edward Elgar Publishing.

Jang, K., S. Kang, J. Kim, C. B. Lee, T. Kim, J. Kim, R. Hirata, and N. Saigusa (2009), Mapping evapotranspiration using MODIS and MM5 Four-Dimensional Data Assimilation, *Remote Sens. Environ.*, *114*(3), 657–673, doi:10.1016/j.rse.2009.11.010.

Kang, S., W. A. Payne, S. R. Evett, C. A. Robinson, and B. A. Stewart (2009), Simulation of winter wheat evapotranspiration in Texas and Henan using three models of differing complexity, *Agric. Water Manage.*, *96*(1), 167–178, doi:10.1016/j.agwat.2008.07.006.

Kiniry, J., M. Schmer, K. Vogel, and R. Mitchell (2008), Switchgrass biomass simulation at diverse sites in the Northern Great Plains of the U.S, *BioEnergy Res.*, *1*(3), 259–264, doi:10.1007/s12155-008-9024-8.

Koster, R. D., and M. J. Suarez (1996), Energy and water balance calculations in the Mosaic LSM, *Tech. Memo Rep. 104606*, 59 pp., NASA.

Koster, R. D., and M. J. Suarez (2003), Impact of land surface initialization on seasonal precipitation and temperature prediction, *J. Hydrometeorol.*, *4*(2), 408–423, doi:10.1175/1525-7541(2003)4<408:IOLSIO>2.0.CO;2.

Koster, R. D., M. J. Suarez, P. Liu, U. Jambor, A. Berg, M. Kistler, R. Reichle, M. Rodell, and J. Famiglietti (2004), Realistic initialization of land surface states: Impacts on subseasonal forecast skill, *J. Hydrometeorol.*, *5*(6), 1049–1063, doi:10.1175/JHM-387.1.

Kovalskyy, V., and G. M. Henebry (2012a), A new concept for simulation of vegetated land surface dynamics – Part 1: The event driven phenology model, *Biogeosci.*, *9*(1), 141–159, doi:10.5194/bg-9-141-2012.

Kovalskyy, V., and G. M. Henebry (2012b), Alternative methods to predict actual evapotranspiration illustrate the importance of accounting for phenol-ogy – Part 2: The event driven phenology model, *Biogeosci.*, *9*(1), 161–177, doi:10.5194/bg-9-161-2012.

Kovalskyy, V., D. P. Roy, X. Y. Zhang, and J. Ju (2011), The suitability of multi-temporal web-enabled Landsat data NDVI for phenological monitoring – A comparison with flux tower and MODIS NDVI, *Remote Sens. Lett.*, *3*(4), 325–334, doi:10.1080/01431161.2011.593581.

Lawrence, P. J., and T. N. Chase (2007), Representing a new MODIS consistent land surface in the Community Land Model (CLM 3.0), *J. Geophys. Res.*, *112*, G01023, doi:10.1029/2006jg000168.

Lewis, P., J. Gómez-Dans, T. Kaminski, J. Settle, T. Quaife, N. Gobron, J. Styles, and M. Berger (2012), An Earth observation land data assimila-tion system (EO-LDAS), *Remote Sens. Environ.*, *120*, 219–235, doi:10.1016/j.rse.2011.12.027.

Li, Z.-L., R. Tang, Z. Wan, Y. Bi, C. Zhou, B. Tang, G. Yan, and X. Zhang (2009), A review of current methodologies for regional evapotranspira-tion estimation from remotely sensed data, *Sens.*, *9*(5), 3801–3853, doi:10.3390/s90503801.

Liu, H., J. Yang, C. Drury, W. Reynolds, C. Tan, Y. Bai, P. He, J. Jin, and G. Hoogenboom (2011), Using the DSSAT-CERES-Maize model to sim-ulate crop yield and nitrogen cycling in fields under long-term continuous maize production, *Nutr. Cycl. Agroecosyst.*, *89*(3), 313–328, doi:10.1007/s10705-010-9396-y.

Luo, L., et al. (2003), Validation of the North American land data assimila-tion system (NLDAS) retrospective forcing over the southern Great Plains, *J. Geophys. Res.*, *108*(D22), 8843, doi:10.1029/2002jd003246.

Manabe, S. (1969), Climate and the ocean circulation, *Mon. Weather Rev.*, *97*(11), 739–774, doi:10.1175/1520-0493(1969)097<0739:CATOC 2.3.CO;2.

Maruyama, A., and T. Kuwagata (2010), Coupling land surface and crop growth models to estimate the effects of changes in the growing season on energy balance and water use of rice paddies, *Agricultural and Forest Meteorology*, *150*(7–8), 919–930, doi:10.1016/j.agrformet.2010.02.011.

Mearns, L. O., T. Mavromatis, E. Tsvetsinskaya, C. Hays, and W. Easterling (1999), Comparative responses of EPIC and CERES crop models to high and low spatial resolution climate change scenarios, *J. Geophys. Res.*, *104*(D6), 6623–6646, doi:10.1029/1998jd200061.

Meng, C. L., Z. L. Li, X. Zhan, J. C. Shi, and C. Y. Liu (2009), Land surface temperature data assimilation and its impact on evapotranspiration esti-mates from the Common Land Model, *Water Resour. Res.*, *45*, W02421, doi:10.1029/2008wr006971.

Miralles, D. G., T. R. H. Holmes, R. A. M. De Jeu, J. H. Gash, A. G. C. A. Meesters, and A. J. Dolman (2010), Global land-surface evaporation esti-mated from satellite-based observations, *Hydrol. Earth Syst. Sci. Discuss.*, *7*(5), 8479–8519, doi:10.5194/hessd-7-8479-2010.

Mitchell, K. E., et al. (2004), The multi-institution North American Land Data Assimilation System (NLDAS): Utilizing multiple GCIP products and partners in a continental distributed hydrological modeling system, *J. Geophys. Res.*, *109*, D07S90, doi:10.1029/2003jd003823.

Monteith, J. L. (1965), Evaporation and environment, paper presented at *Symposium Society Experiment. Biology, 1965*, Cambridge University Press, London, *19*, 205–234.

Mu, Q., F. A. Heinsch, M. Zhao, and S. W. Running (2007), Development of a global evapotranspiration algorithm based on MODIS and global meteorology data, *Remote Sens. Environ.*, *111*(4), 519–536, doi:10.1016/j.rse.2007.04.015.

Mu, Q., L. A. Jones, J. S. Kimball, K. C. McDonald, and S. W. Running (2009), Satellite assessment of land surface evapotranspiration for the pan-Arctic domain, *Water Resour. Res.*, *45*, W09420, doi:10.1029/2008wr007189.

Mu, Q., M. Zhao, and S. W. Running (2011), Improvements to a MODIS global terrestrial evapotranspiration algorithm, *Remote Sens. Environ.*, *115*, 1781–1800, doi:10.1016/j.rse.2011.02.019.

Nagler, P. L., J. Cleverly, E. Glenn, D. Lampkin, A. Huete, and Z. Wan (2005), Predicting riparian evapotranspiration from MODIS vegetation indices and meteorological data, *Remote Sens. Environ.*, *94*(1), 17–30, doi:10.1016/j.rse.2004.08.009.

Nagler, T., H. Rott, P. Malcher, and F. Müller (2008), Assimilation of meteorological and remote sensing data for snowmelt runoff forecasting, *Remote Sens. Environ.*, *112*(4), 1408–1420, doi:10.1016/j.rse.2007.07.006.

Niu, G.-Y., et al. (2011), The community Noah land surface model with multiparameterization options (Noah-MP): 1. Model description and evaluation with local-scale measurements, *J. Geophys. Res.*, *116*, D12109, doi:10.1029/2010jd015139.

Nkomozepi, T., and S.-O. Chung (2012), Assessing the trends and uncertainty of maize net irrigation water requirement estimated from climate change projections for Zimbabwe, *Agric. Water Manage.*, *111*(0), 60–67, doi:10.1016/j.agwat.2012.05.004.

Pitman, A. J. (2003), The evolution of, and revolution in, land surface schemes designed for climate models, *Int. J. Climatol.*, *23*(5), 479–510, doi:10.1002/joc.893.

Prihodko, L., A. S. Denning, N. P. Hanan, I. Baker, and K. Davis (2008), Sensitivity, uncertainty and time dependence of parameters in a complex land surface model, *Agr. Forest. Meteorol.*, *148*(2), 268–287, doi:10.1016/j.agrformet.2007.08.006.

Ransom, J., D. Franzen, P. Glogoza, K. Hellevang, V. Hofman, M. McMullen, and R. Zollinger (2004), Basics of corn production in North Dakota, *North Dakota Extension Service*, 20.

Rosero, E., Z.-L. Yang, L. E. Gulden, G.-Y. Niu, and D. J. Gochis (2009), Evaluating enhanced hydrological representations in Noah LSM over transition zones: Implications for model development, *J. Hydrometeorol.*, *10*(3), 600–622, doi:10.1175/2009JHM1029.1.

Rötzer, T., M. Leuchner, and A. Nunn (2010), Simulating stand climate, phenology, and photosynthesis of a forest stand with a process-based growth model, *Int. J. Biometeorol.*, *54*(4), 449–464, doi:10.1007/s00484-009-0298-0.

Running, S. W., R. R. Nemani, F. A. Heinsch, M. Zhao, M. Reeves, and H. Hashimoto (2004), A continuous satellite-derived measure of global terrestrial primary production, *Bioscience*, *54*(6), 547–560, doi:10.1641/0006-3568(2004)054[0547:acsmog]2.0.co;2.

Sabater, J. M., C. Rüdiger, J.-C. Calvet, N. Fritz, L. Jarlan, and Y. Kerr (2008), Joint assimilation of surface soil moisture and LAI observations into a land surface model, *Agr. Forest. Meteorol.*, *148*(8-9), 1362–1373, doi:10.1016/j.agrformet.2008.04.003.

Schaaf, C. B., et al. (2002), First operational BRDF, albedo nadir reflectance products from MODIS, *Remote Sens. Environ.*, *83*(1-2), 135–148, doi:10.1016/S0034-4257(02)00091-3.

Senay, G. (2008), Modeling landscape evapotranspiration by integrating land surface phenology and a water balance algorithm, *Algorithms*, *1*(2), 52–68, doi:10.3390/a1020052.

Senay, G., M. Budde, J. Verdin, and A. Melesse (2007), A coupled remote sensing and simplified surface energy balance approach to estimate actual evapotranspiration from irrigated fields, *Sens.*, *7*(6), 979–1000, doi:10.3390/s7060979.

Settle, J., and N. Campbell (1998), On the errors of two estimators of subpixel fractional cover when mixing is linear, *Geosci. Remote Sens. IEEE Trans. on*, *36*(1), 163–170, doi:10.1109/36.655326.

Stancalie, G., A. Marica, and L. Toulios (2010), Using Earth observation data and CROPWAT model to estimate the actual crop evapotranspiration, *Phys. Chem. Earth, Parts A/B/C*, *35*(1–2), 25–30, doi:10.1016/j.pce.2010.03.013.

Tucker, C. J. (1979), Red and photographic infrared linear combinations for monitoring vegetation, *Remote Sens. Environ.*, *8*(2), 127–150, doi:10.1016/0034-4257(79)90013-0.

Turner, M. R. J., J. P. Walker, and P. R. Oke (2008), Ensemble member generation for sequential data assimilation, *Remote Sens. Environ.*, *112*(4), 1421–1433, doi:10.1016/j.rse.2007.02.042.

Vinukollu, R. K., E. F. Wood, C. R. Ferguson, and J. B. Fisher (2011), Global estimates of evapotranspiration for climate studies using multisensor remote sensing data: Evaluation of three process-based approaches, *Remote Sens. Environ.*, *115*(3), 801–823, doi:10.1016/j.rse.2010.11.006.

Wegehenkel, M. (2009), Modeling of vegetation dynamics in hydrological models for the assessment of the effects of climate change on evapotranspiration and groundwater recharge, *Adv. Geosci.*, *21*, 109–115, doi:10.5194/adgeo-21-109-2009.

Willmott, C., and K. Matsuura (2007), Terrestrial water budget data archive: Monthly time series (1950–1999) *30*.

Xia, Y., et al. (2012a), Continental-scale water and energy flux analysis and validation for the North American Land Data Assimilation System project phase 2 (NLDAS-2): 1. Intercomparison and application of model products, *J. Geophys. Res. Atmos.*, *117*, D03109, doi:10.1029/2011jd016048.

Xia, Y., et al. (2012b), Continental-scale water and energy flux analysis and validation for North American Land Data Assimilation System project phase 2 (NLDAS-2): 2. Validation of model-simulated streamflow, *J. Geophys. Res. Atmos.*, *117*, D03110, doi:10.1029/2011jd016051.

Yan, H., et al. (2012), Global estimation of evapotranspiration using a leaf area index-based surface energy and water balance model, *Remote Sens. Environ.*, *124*, 581–595, doi:10.1016/j.rse.2012.06.004.

Yuan, W., *et al.* (2010), Global estimates of evapotranspiration and gross primary production based on MODIS and global meteorology data, *Remote Sens. Environ.*, *114*(7), 1416–1431, doi:10.1016/j.rse.2010.01.022.

Zha, T., A. G. Barr, G. van der Kamp, T. A. Black, J. H. McCaughey, and L. B. Flanagan (2010), Interannual variation of evapotranspiration from forest and grassland ecosystems in western Canada in relation to drought, *Agr. Forest. Meteorol.*, *150*(11), 1476–1484, doi:10.1016/j.agrformet.2010.08.003.

Zhang, X., M. A. Friedl, C. B. Schaaf, A. H. Strahler, J. C. F. Hodges, F. Gao, B. C. Reed, and A. Huete (2003), Monitoring vegetation phenology using MODIS, *Remote Sens. Environ.*, *84*(3), 471–475, doi:10.1016/S0034-4257(02)00135-9.

Zhang, X., M. A. Friedl, and C. B. Schaaf (2006), Global vegetation phenology from Moderate Resolution Imaging Spectroradiometer (MODIS): Evaluation of global patterns and comparison with in situ measurements, *J. Geophys. Res.*, *111*, G04017, doi:10.1029/2006jg000217.

Zhang, X., M. A. Friedl, and C. B. Schaaf (2009), Sensitivity of vegetation phenology detection to the temporal resolution of satellite data, *Int. J. Remote Sens.*, *30*(8), 2061–2074, doi:10.1080/01431160802549237.

Zhenzhong, Z., P. Shilong, L. Xin, Y. Guodong, P. Shushi, C. Philippe, and B. M. Ranga (2012), Global evapotranspiration over the past three decades: Estimation based on the water balance equation combined with empirical models, *Environ. Res. Lett.*, *7*(1), 014026, doi:10.1088/1748-9326/7/1/014026.